Journal of Power Sources 191 (2009) 127–133

Contents lists available at ScienceDirect

Journal of Power Sources

journal homepage: www.elsevier.com/locate/jpowsour

Failure modes of valve-regulated lead-acid batteries for electric bicycle applications in deep discharge

Yonglang Guo[a,*], Shengqun Tang[a], Gang Meng[b], Shijun Yang[b]

[a] College of Chemistry and Chemical Engineering, Fuzhou University, Fuzhou 350108, PR China
[b] Hubei Camel Storage Battery Co. Ltd., Gucheng 441705, PR China

ARTICLE INFO

Article history:
Received 26 June 2008
Received in revised form 20 August 2008
Accepted 21 August 2008
Available online 29 August 2008

Keywords:
Cycle life
Electric bicycle
Failure modes
Softening
Valve-regulated lead-acid batteries

ABSTRACT

The 36 or 48 V valve-regulated lead-acid (VRLA) battery packs have been widely applied to the power sources of electric bicycles or light electric scooters in China. The failure modes of the 12 V/10 Ah VRLA batteries have been studied by the cycle life test at C_2 discharge rate and 100% depth of discharge (DOD). It indicates that the main cause of the battery failure in this cycle duty is the softening and shedding of positive active mass (PAM) rather than individual water loss, recombination efficiency or sulfation, etc. When the electrolyte saturation falls to a certain extent, the high oxygen recombination current leads to the depolarization of the negative plate and the shift of the positive plate to a higher potential. The violent oxygen evolution accelerates the softening of PAM and the end of cycle life.

1. Introduction

In the last two decades, much effort has been devoted to the study of valve-regulated lead-acid (VRLA) batteries in the applications of electric vehicles (EV) and hybrid EVs [1–5]. In China, there is a population of more than 1.3 billion. Most people go to work by bicycle and 65.5 million bicycles were produced in 2007. In recent years, however, more and more people use electric bicycles or light electric scooters to substitute for bicycles. These new vehicles have a 250 or 350 W electromotor driven by a 36 or 48 V VRLA battery pack, respectively [5,6]. Based on the power of the electromotor used, the battery capacity is 12 V 10, 17 or 20 Ah. The held amount of the electric bicycles and light electric scooters at least reaches 60 M till the end of last year. It corresponds to about 200 M 12 V/10 Ah VRLA batteries, or about RBM 26 billion. The practical operating life of batteries is normally in the range of 1–2 years. With the rapid development of Chinese or Asian economy, more electric bicycles and their batteries will be needed and they have a huge potential market in the coming years, which also promotes the development of EV.

Although there are many failure modes of VRLA batteries, including premature capacity loss (PCL), grid corrosion, softening, sulfation, drying out, additive decomposition and poor separator-plate contact, etc., they vary with different designs, manufacturing and operating conditions [7–15]. In the deep cycle duty, the interface of the grid/active mass easily accumulates the lead sulfate crystals with very high resistance and forms a barrier layer when Pb–Sb alloys in the positive grid are substituted by Pb–Cd–Sn–Al alloys. It is called the "antimony-free effect" and the PCL-1 failure mode [7,8]. Although the barrier layer can be obviously improved with the application of Sn content more than 1.2 wt.%, it is susceptible to the abuse conditions such as deep discharge. So most manufacturers in China use Pb–Sb–Cd alloys as positive grid. However, Cd is poisonous and must be excluded. The corrosion of positive grids in the cycle duty is not heavy as compared with that in the float applications. The high contents of Ca and Al accelerate the corrosion rate of positive grids greatly, although they have good mechanical properties and castability. The active mass (AM) of positive plates undergoes great volume expansion and shrinkage in the deep cycle duty, which can lead to poor contact between AM particles [8,9]. This is the PCL-2 failure mode often taking place in the EV batteries. It can be greatly improved by compressing the plate stack, optimizing the manufacture technology of positive plates and increasing the ratio of positive to negative AM. The serious sulfation of negative plates often occurs when the battery operates at the high rates in a partial-state-of-charge (HRPSoC) or has a high current of oxygen recombination or when the additives at negative plates are decomposed under the high temperature condition [1,10,11]. It will be overcome with the use of high content graphite

* Corresponding author. Tel.: +86 591 8789 2893; fax: +86 591 8807 3608.
E-mail address: yguo@fzu.edu.cn (Y. Guo).

0378-7753/$ – see front matter © 2008 Elsevier B.V. All rights reserved.
doi:10.1016/j.jpowsour.2008.08.059

in negative active mass (NAM) [12]. Drying out is mostly connected with a high charge voltage and current, often in combination with high battery temperature. In the extreme cases, thermal runaway may take place for a battery with very low electrolyte saturation. Water loss depends on the grid compositions, impurities, battery temperature and charge voltage [8]. The suitable charge regime including fast charge is very important for prolonging the battery cycle life [13]. For the practice operating of electric bicycle batteries, their discharge current depends on the electromotor power and the accelerating processes. The cutoff voltage is 10.5 V. They are normally charged at a current-limited constant voltage (CCCV) (2 A/14.8 V) for one night, two or three times per week. Some chargers also use the multi-step constant current charge. In the standard test, however, the electric bicycle batteries are discharged at a 2 h rate to 70% or 100% depth of discharge (DOD) and charged at the current-limited constant voltage.

Although the VRLA batteries have been widely used in electric bicycle, their cycle life and performance still need to be further improved. In this work, the manufacture technologies of 12 V/10 Ah VRLA batteries were optimized and the failure modes in the deep cycle duty were investigated.

2. Experimental

The test battery was 12 V/10 Ah (C_2 rate) VRLA batteries composed of seven positive and eight negative plates and the absorptive glass mat (AGM) separator. The positive and negative grids were Pb–0.065% Ca–1.2% Sn–0.003% Al and Pb–0.085% Ca–0.35% Sn–0.015% Al alloys, respectively. The positive and negative pastes contained 45 and 42 g H_2SO_4 per kg lead powder. Their apparent densities were 4.3–4.4 g cm^{-3}. It took 48 h for their curing and drying. Then the batteries were assembled and filled with 1.25 g cm^{-3} H_2SO_4 containing 1.5% Na_2SO_4. The container formation was conducted by the multi-step constant current charge regime with two discharge steps within 70 h. The battery weight was about 4.25 kg. In the cycle test, the batteries were discharged at 5 A (C_2 rate) to 10.5 V (100% DOD) and charged at a current-limited constant voltage of 2.5 A/14.4 V for 6 h, followed by charging at 0.8 A for 1 h again at ambient temperature of about 25 °C. The specific energy of the battery reaches 32.6 Wh kg^{-1}. The cycling test was terminated when the battery capacity fell to 7 Ah (70% rate capacity). In order to measure the battery internal resistance, a short current pulse with 5 A and 1 ms was exerted by Arbin BT2000 instruments. After the cycle life test, the batteries were torn down and analyzed. The powder X-ray diffraction (XRD) of positive and negative active mass (PAM and NAM) were carried out by a X' Pert Pro MPD Diffractometer (Philips). Their appearance was observed by a scanning electron microscope (SEM, Philips, XL30ESEM-TEP).

3. Results and discussion

3.1. Cycle tests

Fig. 1 shows the dependence of the discharge capacity of two batteries on cycle number at C_2 discharge rate. In the initial cycles, their capacity increases and reaches the maximum, 11.55 Ah, in the 28th cycle. Then it decreases gradually before the 250th cycle. After that, it becomes relatively stable, but it drops quickly after about the 600th cycle. The cycle life of battery A and B is similar and reaches about 680 cycles.

Since in various failure modes, the grid corrosion, PAM softening, drying out, sulfation or undercharge, etc. are closely related to the battery charge, the charge regime affects the cycle life of the test batteries greatly [16–18]. Fig. 2 shows the changes of the charge

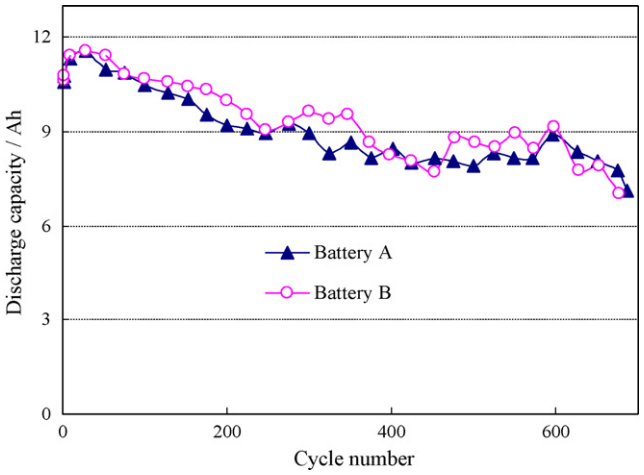

Fig. 1. Evolution of discharge capacity of two batteries in the cycles at 100% DOD.

current and battery voltage at the current-limited constant voltage in the cycle life test. In the first constant current stage (2.5 A), the constant current time in Fig. 2A shortens with the cycles. It is due to the gradual falling of the battery capacity. The rising of the charge voltage in Fig. 2B indicates the increase of the battery polarization resistance due to water loss and battery degeneration, etc. In the second constant voltage stage (14.4 V), the charge current drops

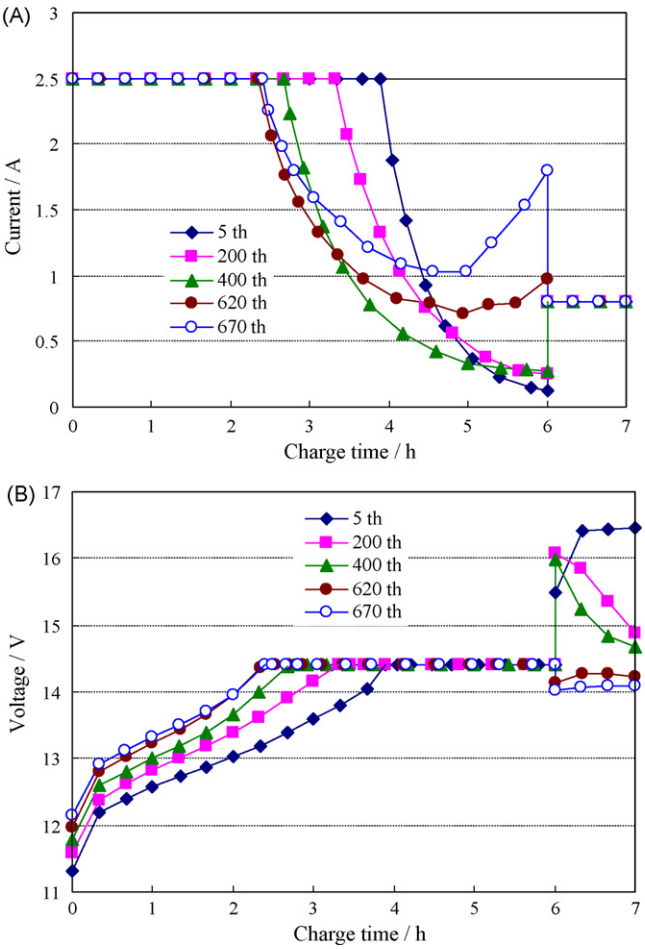

Fig. 2. The changes of (A) charge current and (B) charge voltage at the current-limited constant voltage in different cycles.

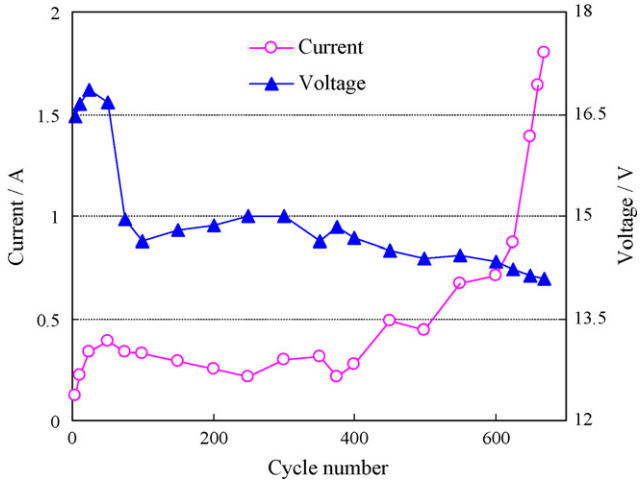

Fig. 3. Evolutions of charge current at 6 h and charge voltage at 7 h in Fig. 2.

quickly and reaches very small value. However, the 'tail' current at 6 h begins to increase obviously after about the 400th cycle and its detail evolution is shown in Fig. 3. At the final stage of charge at 0.8 A, Fig. 2B shows that the charge voltage at first increases and then decreases as the cycle test proceeds. The turning point appears about in the 50th cycle and the charge voltage reaches 16.68 V. Then the maximum charge voltage decreases gradually with the electrolyte consumption or the decrease of the electrolyte saturation, which leads to the depolarization of the negative plate. After the 570th cycle, the maximum charge voltage is lower than 14.40 V. It means that such low polarization may result in the undercharge and the accumulation of $PbSO_4$ at the negative plate.

Fig. 3 shows dependence of the charge current at the end of constant voltage (6 h) in Fig. 2A and the voltage at the end of constant current (7 h) in Fig. 2B on the cycle number. In practice, this charge current responses to the rate of oxygen recombination or charge efficiency and the charge voltage responses to the polarization or effective charge. It is found from Fig. 3 that the battery charge voltage is very high and the charge current increases from 0.12 to 0.39 A in the initial 50 cycles. It indicates that the battery has high electrolyte saturation and very low oxygen recombination current in this period. Then the charge voltage drops very quickly and is stabilized in the range of 14.6–15.0 V till the 400th cycle,

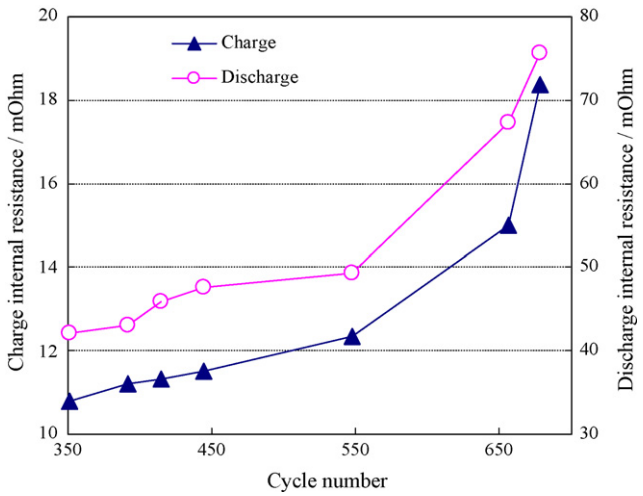

Fig. 4. The changes of the battery internal resistance at the end of charge and discharge in the cycles.

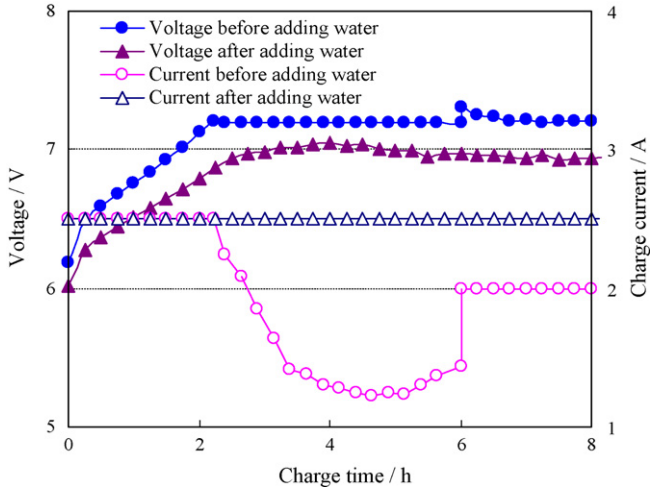

Fig. 5. The changes of voltage and current when the three failed cells were charged before and after adding water.

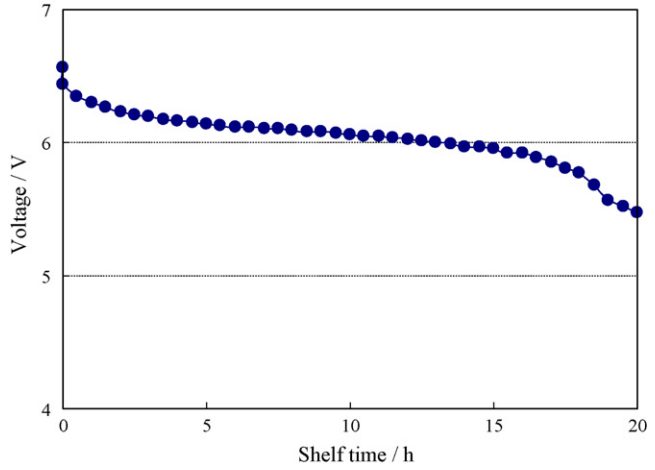

Fig. 6. The voltage falling of three cells during the shelf after adding water and a few cycles.

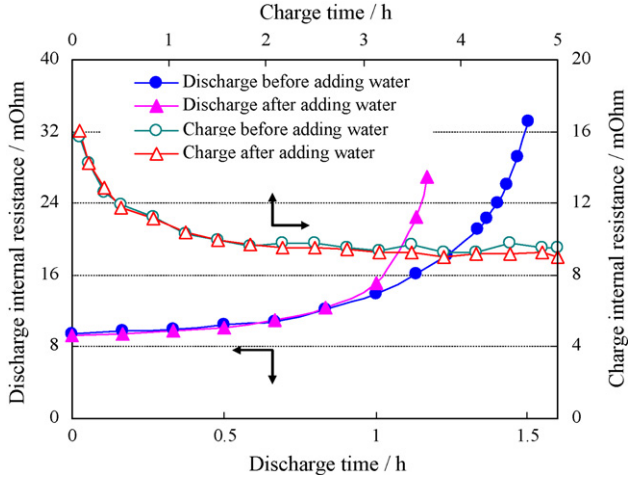

Fig. 7. The changes of the internal resistance in the charge and discharge of three cells before and after adding water.

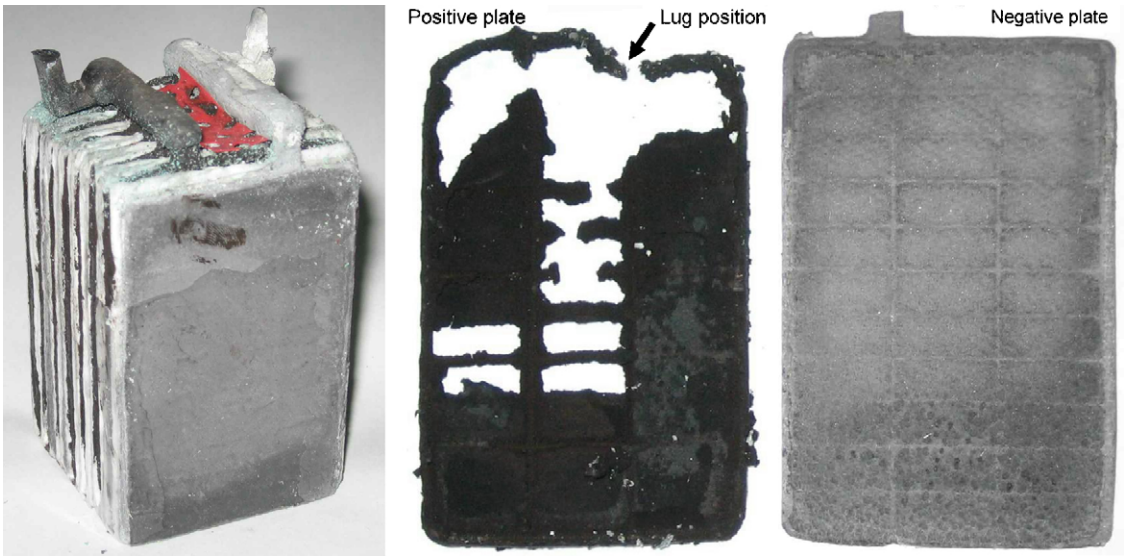

Fig. 8. The photographs of the plate stack and its positive and negative plates of failed battery A.

and the charge current lies in the range of 0.211–0.388 A. This is a relatively ideal cycle process, in which the relatively high voltage not only ensures the full charge and but also no more water loss occurs. After that, especially the 600th cycle later, the charge current at constant voltage stage increases rapidly while the charge voltage decrease gradually from 14.68 to 14.09 V. In this stage, the electrolyte saturation only decreases by 1.2% (from 88.2% to 87.0%) in about 250 cycles. Kirchev and Pavlov [19] found that the liquid film thickness on the surface of NAM and oxygen recombination rate change sharply when the electrolyte saturation is lower than about 87%. At this time, therefore, only a little decrease of the electrolyte saturation will result in very high oxygen recombination current and the depolarization of the negative plate. And the battery undercharge may occur. It also indicates that the battery is difficult to be fully charged at 14.6 V for 7 h charge time, which will lead to the obvious degradation of the batteries in the subsequent cycles.

The battery internal resistance is related to the battery structure, electrolyte saturation, grid corrosion, contact between PAM particles, passivation, AM sulfation and reaction area, etc. Since the internal resistance is small for a new or normally operating battery, the changes of the battery internal resistance at the end of charge and discharge were measured only in the later half of cycle life test and shown in Fig. 4. The discharge resistance is about four

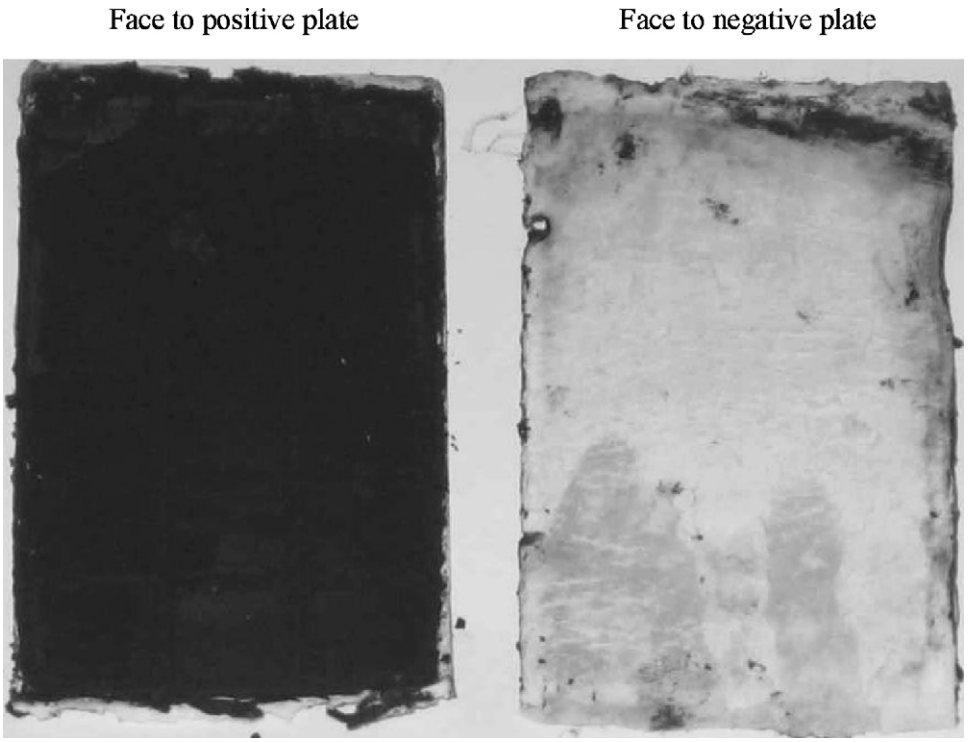

Fig. 9. The torn-down AGM separator from the failed battery.

times the charge resistance. And their resistance increases greatly after the 550th cycle, especially the final 20 cycles. Apparently, the battery failure is closely related to the rapid rising of the internal resistance. It can be seen from Fig. 3 that the oxygen recombination current goes up sharply in the period. This further leads to the depolarization of the negative plate, the shift of the positive plate to higher potential and more violent evolution of oxygen. As a result, the contact between PAM particles becomes poor and the resistance increases rapidly, which can accelerate the battery capacity falling and the end of the cycle life.

3.2. Overcharge and adding water tests

The C_2 capacity of battery A was only 6.03 Ah after 700 cycles. In order to analyze the causes of the battery failure, the battery was divided into two 6 V batteries (three cells) after the end of the cycle life. They went through the overcharge, adding water and resistance measurements. Since the charge current at the constant voltage of 14.4 V has reached 1.8 A in the 670th cycle in Fig. 2A, the subsequent constant charge of 0.8 A cannot make the battery fully charged. To see whether the battery is undercharged, the final 0.8 A 1 h charge was changed into 2 A 2 h charge and two cycles were performed. The first charge amount is 2.53 times the previous discharge capacity, but the next discharge capacity is only 6.45 Ah and has the comeback of only 7% capacity. In order to know whether the battery failure is due to excessive water loss, each cell was filled with about 18 ml water after the battery was fully charged. The second C_2 capacity is only 5.58 Ah, less than the first capacity. It indicates that the water loss and undercharge are not the major causes of the battery failure.

Fig. 5 shows the changes of the charge current and voltage before and after adding water mentioned above. Before adding water, their curves are normal. But after adding water, the maximum charge voltage only reaches 2.349 V per cell so that the charge current always keeps the limited value of 2.5 A. Based on the charge voltage at 2.5 A for a 'flood' lead-acid battery, it can be presumed that the internal short circuit takes place in the battery. Fig. 6 shows the voltage decline of the fully charged battery during its shelf. Its capacity was completely self-discharged within 20 h. The H_2SO_4 solution after charging shows a little black color, instead of being transparent. It indicates that severe softening occurs at the positive plate. A lot of PAM particles shed and enter into the electrolyte at high charge current. These PbO_2 particles can be precipitated at the negative plate as dendritic lead which passes through the AGM separator to form the tiny short circuit.

Fig. 7 shows the changes of the internal resistance in the charge and discharge of the three failed cells before and after adding water. During charging, the internal resistance decreases gradually and two curves are the same. During discharging, the internal resistance increases sharply at the end and it is greatly affected by adding water. The battery capacity decreases from 7.50 to 5.83 Ah. So similar to the results above, the battery failure is not caused by water loss. On the contrary, the addition of water hinders the oxygen escape from the micropores in PAM during overcharging, which can increase the internal pressure in PAM and may cause its shedding. After another three cycles, the charge voltage of the three cells

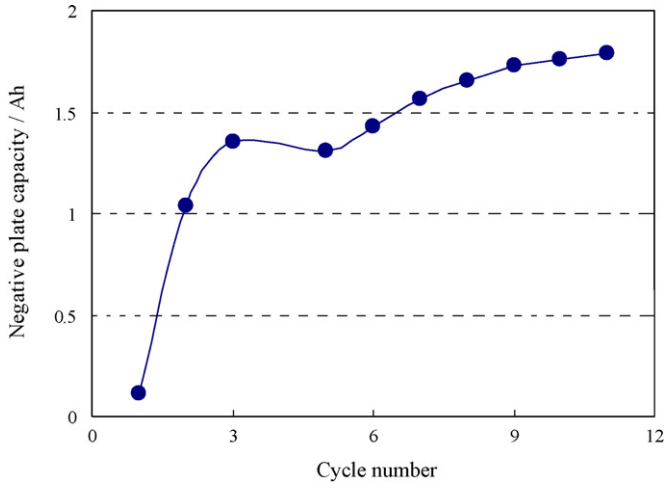

Fig. 10. The capacity comeback of the negative plate of the failed battery in the cycles.

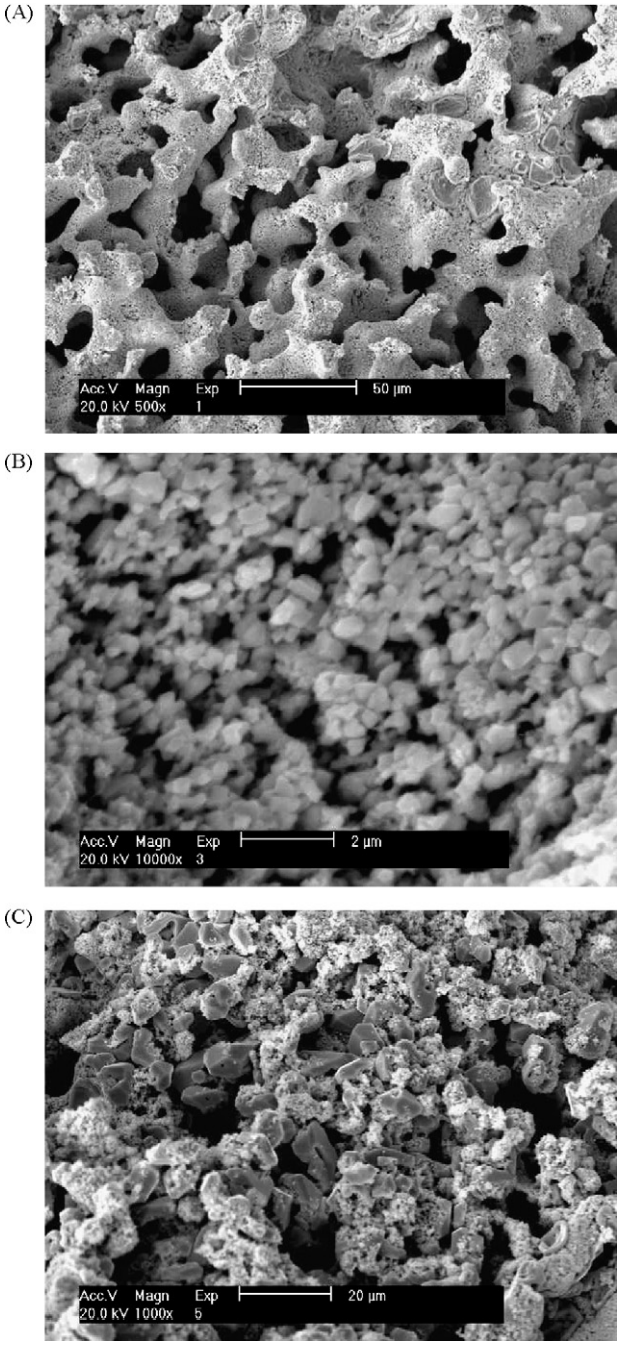

Fig. 11. SEM of active mass in different parts of positive plate of the failed battery. (A) 500×, (B) 10,000× and (C) 1000×.

only reaches 6.72 V at the constant current of 2.5 A. So the internal short circuit can also take place.

3.3. Teardown analysis

Battery A was torn down after the cycle life test was ended. Fig. 8 shows the photographs of the plate stack and its positive and negative plates. The plate stack and negative plate had the integrated structures. Although some ribs of the positive grid were severely corroded, its frame was still well and the positive plate had relatively good mechanical property. It is found, however, that the severe softening appears in PAM, especially in the upper part of the positive plate. Fig. 9 indicates that the AGM separator facing positive plate glues a lot of PAM particles and that the AGM separator facing negative plate is normal. This is due to the fact that the PAM particles become increasingly small with the cycles and their contact among one another becomes poor, resulting in the softening and shedding.

In order to know whether the negative plate fails, one negative plate of the failed battery was placed between two normal positive plates, separated by PE separator, and they were put into excessive H_2SO_4 solution of 1.28 specific gravity. And then the cell was cycled according to the conditions of the cycle life test. That is, charge at 0.36 A 2.4 V for 6 h and at constant current of 0.114 A for another 1 h, then discharge to the negative potential of −0.8 V (vs. Hg_2SO_4/Hg) at 0.7 A. Fig. 10 shows the capacity comeback of the negative plate in the cycles. The very low capacity in the first discharge is because the negative plate was in a discharge state when the battery was torn down. It is found that the capacity of the negative plate can come back easily in several cycles. Therefore, the battery failure is not due to the sulfation or passivation of the negative plate.

The SEM of the fully charged PAM of failure battery A are shown in Fig. 11. Fig. 11A shows the typical coralloid structure of PAM. The size of big pores is in the range of 10–20 μm. There are also a lot of micropores on the framework. Fig. 11B is an enlarged Fig. 11A, which indicates that size of the PAM particles is 0.3–0.5 μm and their contact among one another is very poor. The PAM has a high crystallinity and has lost its hydrated structure, which is unfavorable to the battery capacity and its cycle life. Fig. 11C shows the SEM of PAM in the other position. There are some particles with poor crystallinity or hydrated structure and some large crystals with high crystallinity and 7–8 μm in size, which are $PbSO_4$ crystals. Therefore, the PAM has two structures. One is the accumulation of some $PbSO_4$ crystals. The other is the coralloid structure with poor contact among AM particles. The PAM has softened and shed obviously.

Fig. 12 shows the SEM of the fully charged NAM in the upper and lower parts of the negative plate. It can be seen that there are two structures. They are $PbSO_4$ and Pb crystals. The former are perfect crystals and the latter have a spongy or dendritic structure. Although the NAM is fully charged, the oxygen recombination at the negative plates causes the $PbSO_4$ accumulation. It is found that the $PbSO_4$ crystals in the upper part of the negative plate are a little larger as compared with those in the lower part. This is due to the continual cycle test in which more AM is charged and discharged in the lower part when the electrolyte stratification occurs. In the upper part, on the other hand, more oxygen recombination takes place, in which bigger $PbSO_4$ crystals can be formed by electrochemical and chemical reaction processes [20]. For the practical VRLA batteries with electrolyte stratification, however, the sulfa-

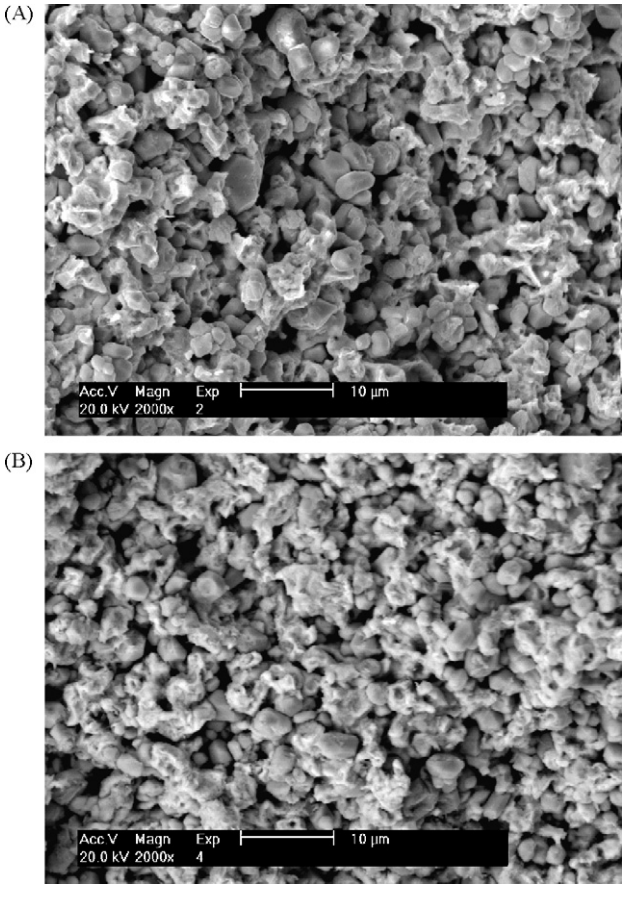

Fig. 12. SEM of active mass in (A) the upper and (B) lower parts of negative plate of the failed battery. (A) 2000× and (B) 2000×.

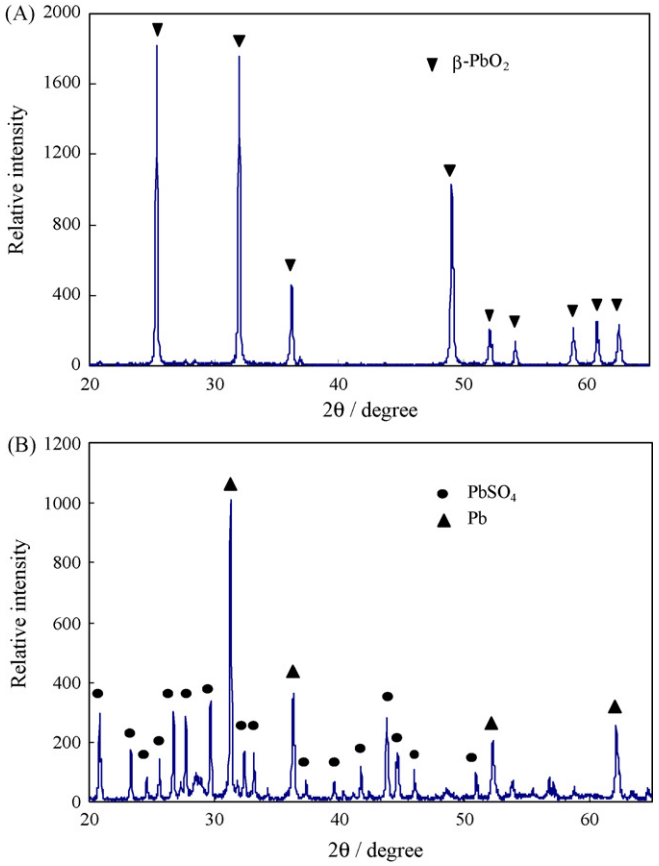

Fig. 13. The XRD patterns of (A) PAM and (B) NAM of the failed battery.

tion or big $PbSO_4$ crystals normally appear in the lower part because of its self-discharge [21]. Therefore, this test battery only has very light electrolyte stratification due to its small plates.

It is well known that the AM of the freshly formed positive and negative plates mainly consists of α/β-PbO_2 and Pb, respectively [22,23]. After the end of cycle life test, Fig. 13 shows their XRD patterns of PAM and NAM in a fully charged state. There are only β-PbO_2 diffraction peaks in PAM in Fig. 13A. No α-PbO_2 and $PbSO_4$ are observed due to the resolution of XRD diffractometer. The chemical analysis indicates that the content of PbO_2 in AM of the torn-down positive plate reaches 89%. Therefore, the content of $PbSO_4$ is very low in PAM although it is found in Fig. 11C. At the negative plate, however, there are a lot of $PbSO_4$ crystals besides spongy lead. The chemical analysis also shows 36% $PbSO_4$ were found in NAM. All this is attributed to the very high current of oxygen recombination.

4. Conclusions

In this work, a 12 V/10 Ah VRLA battery in the electric bicycle applications was designed and manufactured. The cycle test was conducted at C_2 discharge rate and 100% DOD. The measurement and teardown analysis for the failure battery indicate that the battery failure is not due to individual water loss, grid corrosion, electrolyte stratification, recombination efficiency or sulfation. The main cause is the softening and shedding of PAM. When the electrolyte saturation falls to a certain extent, the oxygen recombination current increases rapidly with the cycles, which leads to the depolarization of the negative plate and the shift of the positive plate to a higher potential. Consequently, the oxygen evolution becomes increasingly violent, the contact among PAM particles becomes poor and the softening is accelerated. Although many $PbSO_4$ are found in NAM due to oxygen recombination, they do not passivate the negative plate and can be reduced when the polarization of the negative electrode increases.

Acknowledgements

The authors are grateful to Natural Science Foundation of Fujian Province (no. E0510006) for financial support for this work.

References

[1] P.T. Moseley, B. Bonnet, A. Cooper, M.J. Kellaway, J. Power Sources 174 (2007) 49–53.
[2] W.X. Shen, Energy Conv. Manage. 48 (2007) 433–442.
[3] H. Blanke, O. Bohlen, S. Buller, R.W. De Doncker, B. Fricke, A. Hammouche, D. Linzen, M. Thele, D.U. Sauer, J. Power Sources 144 (2005) 418–425.
[4] M.L. Soria, F. Trinidad, J.M. Lacadena, A. Sánchez, J. Valenciano, J. Power Sources 168 (2007) 12–21.
[5] W. Ke, N. Zhang, 2007 Second IEEE Conference on Industrial Electronics and Applications, 2007, pp. 1370–1373.
[6] F. Pei, X. Huang, Y. Luo, K. Zhao, Proc. Chin. Soc. Electr. Eng. 25 (9) (2005) 164–168.
[7] A. Cooper, P.T. Moseley, J. Power Sources 113 (2003) 200–208.
[8] R. Wagner, J. Power Sources 53 (1995) 153–162.
[9] K. Nakamura, M. Shiomi, K. Takahashi, M. Tsubota, J. Power Sources 59 (1996) 153–157.
[10] L.T. Lam, N.P. Haigh, C.G. Phyland, A.J. Urban, J. Power Sources 133 (2004) 126–134.
[11] S. Atlung, B.Z. Christiansen, J. Power Sources 52 (1994) 201–209.
[12] R.H. Newnham, W.G.A. Balding, A.F. Hollenkamp, O.V. Lim, C.G. Phyland, D.A.J. Rand, J.M. Rosalie, D.G. Vella, ALABC Project C/N 1.1, Advancement of valve-regulated lead-acid battery technology for hybrid-electric and electric vehicles, Semi-annual Report 1 July to 31 December 2001, Advanced Lead-Acid Battery Consortium, Research Triangle Park, NC, USA, 2001.
[13] T.G. Chang, D.M. Jochim, J. Power Sources 91 (2000) 177–192.
[14] Y. Yamaguchi, K. Hirakawa, E. Hojo, Y. Nakayama, INTELEC, 2001, pp. 369–375.
[15] B. Culpin, D.A.J. Rand, J. Power Sources 36 (1991) 415–438.
[16] M. Dimitrov, D. Pavlov, J. Power Sources 93 (2001) 234–257.
[17] R.F. Nelson, E.D. Sexton, J.B. Olson, M. Keyser, A. Pesaran, J. Power Sources 88 (2000) 44–52.
[18] M. Fernandez, F. Trinidad, J. Valenciano, A. Sanchez, J. Power Sources 158 (2006) 1149–1165.
[19] A. Kirchev, D. Pavlov, J. Power Sources 162 (2006) 864–869.
[20] D.M. Bernardi, M.K. Carpenter, J. Electrochem. Soc. 142 (1995) 2631–2642.
[21] Y. Guo, W. Yan, J. Hu, J. Electrochem. Soc. 154 (2007) A1–A6.
[22] D. Pavlov, G. Papazov, V. Iliev, J. Electrochem. Soc. 119 (1972) 8–19.
[23] D. Pavlov, V. Iliev, J. Power Sources 7 (1981/1982) 153–164.